ATF4 regulates arsenic trioxide-mediated NADPH oxidase, ER-mitochondrial crosstalk and apoptosis

Ritesh K Srivastava[a], **Changzhao Li**[a], **Aftab Ahmad**[b], **Onika Abrams**[C], **Marina S. Gorbatyuk**[d], **Kevin S. Harrod**[b], **Ronald C. Wek**[e], **Farrukh Afaq**[a], and **Mohammad Athar**[a,#]

[a]Department of Dermatology, University of Alabama at Birmingham, Birmingham, Alabama, USA

[b]Department of Anesthesiology and Perioperative Medicine, University of Alabama at Birmingham, Birmingham, Alabama, USA

[C]Stillman College, 3601 Stillman Blvd. Tuscaloosa, Alabama, USA

[d]Department of Visual Science, University of Alabama at Birmingham, Birmingham, Alabama, USA

[e]Department of Biochemistry and Molecular Biology, Indiana University School of Medicine, Indianapolis, Indiana, USA

Abstract

Arsenic is a mitochondrial toxin, and its derivatives, such as arsenic trioxide (ATO), can trigger endoplasmic reticulum (ER) and the associated unfolded protein response (UPR). Here, we show that arsenic induction of the UPR triggers ATF4, which is involved in regulating this ER-mitochondrial crosstalk that is important for the molecular pathogenesis of arsenic toxicity. Employing $ATF4^{+/+}$ and $ATF4^{-/-}$ MEFs, we show that ATO induces UPR and impairs mitochondrial integrity in $ATF4^{+/+}$ MEF cells which is largely ablated upon loss of ATF4. Following ATO treatment, ATF4 activates NADPH oxidase by promoting assembly of the enzyme components Rac-1/P47^{phox}/P67^{phox}, which generates ROS/superoxides. Furthermore, ATF4 is required for triggering Ca^{++}/calpain/caspase-12-mediated apoptosis following ATO treatment. The IP3R inhibitor attenuates Ca^{++}/calpain-dependent apoptosis, as well as reduces m-ROS and MMP disruption, suggesting that ER-mitochondria crosstalk involves IP3R-regulated Ca^{++} signaling. Blockade of m-Ca^{++} entry by inhibiting m-VDAC reduces ATO-mediated UPR in $ATF4^{+/+}$ cells. Additionally, ATO treatment leads to p53-regulated mitochondrial apoptosis, where p53 phosphorylation plays a key role. Together, these findings indicate that ATO-mediated apoptosis is regulated by both ER and mitochondria events that are facilitated by ATF4 and the UPR. Thus, we describe novel mechanisms by which ATO orchestrates cytotoxic responses involving interplay of ER and mitochondria.
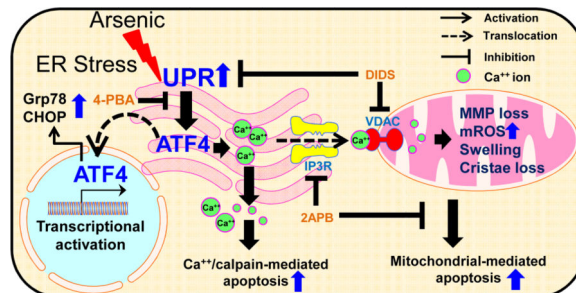
[#]**Corresponding Author:** Mohammad Athar, Ph.D., Department of Dermatology, University of Alabama at Birmingham, 1530 3rd Avenue South, VH 509, Birmingham, AL, 35294-0019, USA. Tel: (205) 975-2616, Fax: 205-934-7554, mathar@uab.edu.

Conflict of interest

The authors disclose that there is no conflict of interest.

Graphical abstract

Keywords

Apoptosis; Arsenic; ATF4; Ca^{++} release; ER-mitochondria crosstalk

1. Introduction

Arsenic is a naturally occurring toxic metalloid that is a widespread contaminant in various regions of the world [1]. In the environment, arsenic can occur as either inorganic or organic forms, with certain inorganic forms being more toxic and persistent [2]. Chronic exposure to inorganic arsenic is associated with development of various cancers affecting skin, lungs, bladder, colon and liver cancer *etc.* [3, 4]. Acute exposure of arsenic has been linked to the induction of multiple stress signaling pathways, which can trigger cell death in many cell types [5].

Both in humans and in experimental animals, sustained activation of cell stress responses that can feature oxidative damages, metabolic alterations, and growth inhibition cause morbidity and mortality [5, 6]. Arsenic mediated-induction of multiple signaling pathways involves increased generation of reactive oxygen species (ROS) that may trigger cell death through the mitochondrial regulated signaling pathways. In this regard, we and others have shown that arsenic-induced ROS disrupt mitochondrial membrane potential (MMP) and mitochondrial functions [7-9], ultimately leading to mitochondrial-regulated cell death [10]. In addition, arsenic-mediated endoplasmic reticulum (ER) stress that activates the unfolded protein response (UPR) signaling and Ca^{++} homeostasis imbalances may play a critical role in the regulation of cell death [11, 12]. The UPR directs transcriptional and translational modes of gene expression that function to ameliorate cell damage and expand the processing capacity of the ER [13]. Central to the UPR program of gene expression is the ATF4 transcription factor that targets genes involved in antioxidation, metabolism, and apoptosis.

Although these stress responses, such as those directed by the UPR, are ubiquitous among different tissues, their ultimate effects on viability may be cell-context dependent. For example, we recently showed that arsenic trioxide (ATO) activates ER stress and UPR signaling in mouse macrophage Raw 264.7 cells, leading to impaired macrophage and innate immune functions [14]. In addition to toxicants, mitochondrial dysfunction has also been shown to contribute to the pathogenesis of many diseases that feature ER stress. For example, Malhotra et al., showed both *in vitro* and *in vivo* that misfolding of newly

synthesized coagulation factor VIII (FVIII), a protein deficient in hemophilia A, activates UPR, which causes oxidative stress and induces apoptosis [15]. Similarly, ER-mitochondria pathobiology has been shown to be associated with β-cell dysfunction and peripheral insulin resistance in Type 2 diabetes mellitus [16, 17].

In this study, we employed syngeneic $ATF4^{+/+}$ and $ATF4^{-/-}$ mouse embryonic fibroblast (MEFs) and showed that ATO-induced UPR signaling at the ER regulates mitochondrial integrity. We found that ATO induces both biochemical and morphological changes in mitochondria only in $ATF4^{+/+}$ cells, whereas $ATF4^{-/-}$ cells remain largely non-responsive to ATO. Of importance, ATF4-dependent activation of NADPH oxidase is central for augmenting ROS generation. This is done in part through Ca^{++} release from ER lumen via inositol trisphosphate receptor (IP3R) phosphorylation. Thus, blocking Ca^{++} release by Ca^{++} channel blockers or Ca^{++}-specific chelators attenuates ATO-mediated toxicity. ATF4 also regulates mitochondrial responses via regulation of the voltage-dependent anion channel (VDAC), which is involved in Ca^{++}-directed MMP regulation and production of mitochondrial ROS (mROS). Attenuation of VDAC-regulated responses restores ER-regulated UPR signaling. Together, this study indicates that ATF4 is required for ATO-mediated alterations in ER–mitochondrial crosstalk via Ca^{++} homeostasis.

2. Materials and methods

2.1. Cell culture and treatments

$ATF4^{+/+}$ and $ATF4^{-/-}$ MEF cells were cultured in the presence of 1% non-essential amino acid and 50 μM β-mercaptoethenol in DMEM medium at 37^0C in a CO_2 incubator. MEFs were exposed to either saline (control) or ATO at concentrations (1-10 μM) for up to 24 h. 2-aminoethyl diphenylborinate (2-APB) (20 μM, 6 h), 4-phenylbutyric acid (4-PBA) (1 mM, 6 h), BAPTA-AM (5 μM, 6h), 4-chlorophenoxy) acetamide, trans-N,N′-1,4-cyclohexanediylbis[2-(4-chlorophenoxy)-acetamide (ISRIB) (200 nM, 6h), superoxide dismutase (SOD) (50 unit/ml), MnTABP (50μM, 6h), 4, 4'-diisothiocyano-2,2'-stilbenedisulfonic acid (DIDS) (200 μM, 6h), thapsigargin (TG) (2.5 M, 3 h), and 4'-hydroxy-3'-methoxyacetophenone (apocynin) (100 μM, 6 h) were used as a pre-treatment in cell culture studies.

2.2. MTT assay

ATO concentrations for this study were selected on the basis of their effects on cell viability in MTT assays. ATO-treated cells were washed with PBS and incubated with MTT (0.5 mg/ml) (Sigma, St. Louis, MO) dye for 3 h at 37°C. At the end of incubation period, the reaction mixture was replaced with 200 l of dimethyl sulfoxide and plates were read at 490 nm using 1420 multilable counter VICTOR3 (Perkin Elmer, Shelton, CT) as described [14]. Saline-treated sets of cells were also run under identical conditions and served as basal control.

2.3. Morphological changes

Morphological changes were assessed in either saline or ATO-treated cultured MEFs and observed for any phenotypic alterations such as cell roundness, cell adhesion loss, and cell

blebbing. Cells were visualized by a Olympus BX51TRF microscope and images were obtained using an Olympus DP71 digital camera (Tokyo, Japan).

2.4. Fractional studies

Cytoplasmic and mitochondrial fractions from *ATF4*+/+ and *ATF4*−/− MEFs was prepared as described [18]. Briefly, harvested cells were suspended in ice-cold cell homogenization medium (150mM $MgCl_2$, 10mM Kcl, 10mM Tris.Cl, pH-6.7). After homogenization, nuclei were pelleted by centrifugation for 5 min at 1000xg. Supernatant was then subjected to centrifugation at 5000xg to isolate mitochondria. Mitochondrial pellet was suspended in mitochondrial suspension medium (0.25M sucrose, 10mM Tris-base, pH 7) and processed for protein quantification and western blot analyses.

2.5. Immunofluorescence staining

Following ATO treatment, MEFs were washed with PBS, fixed in 4 % paraformaldehyde, and permeabilized with 0.1% Triton X-100. Cells were blocked for 1 h with 2% bovine serum albumin. Cells were then incubated with the following primary antibodies: Rac-1 (1:100, Santa Cruz, SC-95), ATF4 (1:100 Cell Signaling-11815), CHOP (1:100, Cell Signaling-2895) or cytochrome-c (1:100, Santa Cruz, SC-13156) overnight at 4°C. After PBS washes, cells were incubated with fluorescein-conjugated secondary antibodies for 1-1.5 h at room temperature. Labeled cells were visualized by fluorescence microscopy (Olympus1X-S8F2, Japan) or confocal microscopy (Zeiss LSM 710 confocal software 63X water corrected objective). In some experiments, cells were stained with mitotracker red (Sigma, St. Louis, MO) or wheat germ agglutinin dye (Invitrogen, Carlsbad, CA) before fixing to stain mitochondria or plasma membrane, respectively.

2.6. Cellular reactive oxygen species (ROS)/superoxide detection

ROS levels were measured by using DCFH-DA probe and the cellular ROS/superoxide assay kit (Abcam, Cambridge, MA). The Abcam ROS/superoxide assay kit includes two fluorescent dyes, which are designed to detect oxidative stress by fluorescent detection reagent (green) for overall ROS and superoxide (O_2^-) generation by specific fluorescent reagents. We employed two different methods for recording ROS/O_2^- radicals that were assayed by ELISA-based plate reader assay and fluorescence-based microscopic image analysis. These experiments incorporated inhibitors of O_2^- radicals, including SOD and SOD mimic, MnTABP, as indicated. For ELISA-based assays, 10,000 cells/well were seeded onto 96-well black bottom plates. Following ATO treatment with or without SOD or MnTABP, cells were washed with PBS and labeled with O_2^- detection reagent for 30 min according to the manufacturer's instructions. Mean fluorescence intensity of O_2^- radicals was recorded at Ex/Em = 550/620 nm and presented as percent change compared to control. For microscopic image analysis, 30,000 cell/well were grown on a coverslip. Following various treatments, cells were washed with PBS and labeled with O_2^- detection reagent for 30 min at 37 °C. Cells were washed again with PBS and visualized by fluorescent microscopy (Olympus1X-S8F2, Japan).

Similarly, overall ROS were detected using DCFH-DA probe by both ELISA-based plate reader assay and microscopic analysis. Following ATO treatment with or without NADPH

oxidase inhibitors apocynin, MEFs were washed with PBS and labeled with DCFH-DA probe. Mean fluorescence intensity was recorded at Ex/Em= 485/535 nm and presented as percent change compared to control. Saline-treated sets were also run in parallel under identical conditions and served as controls.

2.7. Mitochondrial ROS (mROS)

mROS was assessed by the Elite™ mitochondrial ROS activity assay kit (eEnzyme, Gaithersburg, MD). Elite™ ROS orange is a membrane permeable non-fluorescent ROS sensor that rapidly penetrates into mitochondria and generates very strong fluorescence signals upon reacting with O_2^- or hydroxyl radicals. Using this kit, mROS was measured by using a ELISA-based plate reader assay, as well as through fluorescent image analysis. Briefly, for plate reader assays, cells were seeded onto 96-well black bottom plates at density 10,000 cells/well. Following the indicated stress treatments, MEFs were labeled with Elite™ mROS orange stain for 30 min at 37 °C as described in the manufacturer's instruction manual. Fluorescence intensity was measured at Ex/Em=540/570 nm. As controls, saline-treated sets were also analyzed during identical conditions.

Image analysis for mROS production in cells grown on a cover slip was performed using fluorescence microscopy. Following the indicated treatments, cells were washed with PBS and labeled with Elite™ ROS orange stain for 30 min at 37 °C. Cells were washed again with PBS and visualized under fluorescent microscope equipped with TRITC filter set.

2.8. Detection of Ca++ levels

Fluo-4 direct calcium assay kit was used to determine intracellular Ca^{++} levels in saline vs. ATO (2 & 5μM, 14h)-treated MEFs following the instructions provided by the manufacturer (Invitrogen, Carlsbad, CA). Fluorescence at excitation wavelength 494 nm and 516 nm was recorded and expressed as relative fluorescence intensity (RFU). Additionally, image analysis of Ca^{++} release was performed according to manufacturer instruction using fluorescence microscopy.

2.9. Mitochondrial membrane potential (MMP)

MMP was detected using a cationic dye JC-1 (Sigma, St. Lousi, MO). In intact mitochondria, JC-1 forms aggregates and emit red fluorescence, whereas loss of MMP leads to accumulation of JC-1 monomer that emit green fluorescence. After various treatments, cells were incubated with JC-1 dye (10 μM) for 15 min at 37°C followed by PBS wash. Cells were imaged and analyzed with fluorescence microscopy to assess changes in the ratio of red to green fluorescence.

2.10. Transmission Electron Microscopy (TEM)

TEM analysis was performed as described earlier [19]. In brief, $ATF4^{+/+}$ and $ATF4^{-/-}$ MEFs were treated with ATO and then fixed with 2% paraformaldehyde and 2.5% glutaraldehyde in a solution of 0.1 M cacodylate buffer. Cells were then placed in a ice-cold solution of 1% osmium tetraoxide (EMS, Hatfield, PA), 0.8% potassium tetraoxide, and 3 mM calcium chloride. Ultrathin sections were prepared using a Reichert-Ultracut E ultramicrotome and

supported on copper grids/75 mesh, followed by Sato lead stain. Stained sections were imaged using a Tecnai Spirit Twin 20-120 kv electron microscope (FEI, Hillsboro, OR).

2.11. Protein quantification and western blot analysis

Protein assays were carried out using a DC kit (Bio-Rad, Hercules, CA). Equal amounts of protein in whole cell lysates were mixed with 4X laemmli sample buffer (Bio-Rad, Hercules, CA), boiled for 5 minute at 95°C, and resolved by SDS-PAGE. Proteins were then electrophoretically transferred to polyvinylidene difluoride (PVDF) membranes and incubated with primary antibodies i.e. GRP78 (1:1000, Cat no. 3177), GRP94 (1:800, Cat no. 20292), p-PERK (1:1000, Cat no. 3179), ATF4 (1:1000, Cat no. 11815), CHOP (1:1000, Cat no. 2895), p-eIF2α (1:1000, Cat no. 3398), t-eIF2α (1:1000, Cat no. 5324), p-IP3R (1:800, Cat no. 8548), cleaved caspase-3 (1:1000, Cat no. 9661), calpian-1 (1:1000, Cat no. 2556), cleaved caspase-12 (1:800, Cat no.2202), Rac-1 (1:500, Cat no. SC-95), P47phox (1:500, Cat no. SC-14015), P76phox (1:1000, Cat no. 3923), GRP75 (1:1000, Cat no. 3593), Bax (1:1000, Cat no. 2772), Cytochrome C (1:1000, Cat no. 4272), p-p53 (1:1000, Cat no. 9286), p53 (1:1000, Cat no. 2527), VDAC (1:1000, Cat no. 4866), α-β tubulin (1:1000, Cat no. 2148), β- actin (1:5000) p-DRP-1 (S616, Cat no. 4494) ,or pDRP-1 (S637, Cat no. 4867) (1:1000 dilution) for overnight at 4°C. All the antibodies for western blots were purchased from Cell signaling technology (Danvers, MA), except for the preparation against β-actin (Sigma, St. Louis, MO), Rac-1 and P47phox (Santa Cruz, Dallas, TX). Membranes were washed and then incubated with HRP conjugated secondary antibody. Blots were developed with enhanced chemiluminescence according to manufacturer's instructions (Amersham Bioscience, Piscataway, NJ).

2.12. Statistical analysis

Data are expressed as mean ± standard error of mean (SEM). Data were analyzed for statistical significance using one-way analysis of variance (ANOVA) followed by either Dunnett's or Bonferroni post-hoc test to compare multiple groups. The statistical analyses were performed using GraphPad Prism 7. $P<0.05$ was considered to be statistically significant. *- significant compared to controls. # - significant compared to ATO.

3. Results

3.1. ATO alters cell viability in a ATF4-dependent manner

$ATF4^{+/+}$ and $ATF4^{-/-}$ MEF cells show the expected differences in genetic ablation for this transcription factor (Fig. 1A). To determine the suitable ATO doses and exposure times for altered cells viability, we conducted MTT assays at concentrations (1-10 μM) of ATO for 24 h (Supplementary Fig. S1). From this MTT data, we selected 2 and 5 μM concentrations of ATO, which had significant differential viability effects on these MEF cells. While these concentrations manifested multiple morphological and molecular alterations in $ATF4^{+/+}$ MEFs, the $ATF4$-deficient ($ATF4^{-/-}$) cells were resistant. Phenotypic changes observed by ATO treatments included cell rounding, loss of cell adhesion, and blebbing, which were readily visible at 24 h (Fig. 1B). These findings demonstrated that ATO impairs cell viability and morphological alterations in $ATF4^{+/+}$ cells in a concentration-dependent manner, whereas $ATF4^{-/-}$ cells were resistant to these effects of ATO.

3.2. ATO-induced ROS/superoxide generation requires ATF4 and is regulated by the activation of NADPH-oxidase

Superoxide anions are generated in cells by both enzymatic and non-enzymatic mechanisms and are known to play an important role in tissue injury [20]. Our immunofluorescence and ELISA-based assays showed that ATO induces superoxide radicals more efficiently in $ATF4^{+/+}$ as compared to $ATF4$-depleted cells (Fig. 1C.I & 1C.II). Generation of O_2^- following ATO exposure could be blocked by treating cells with permeable SOD or SOD mimetic, MnTABP (Fig. 1D), demonstrating specificity of the assay. These results further demonstrate that ATO-induced ROS/superoxide production occurs primarily through the activation of NADPH oxidase complex in $ATF4^{+/+}$ but not in ATF4-depleted cells.

NADPH oxidase consists of three cytosolic components (p67^{phox}, p47^{phox} and p40^{phox}), two membrane-bound elements (gp91^{phox} and p22^{phox}), and a low-molecular-weight G protein (Rac-1) [21]. Activation of NADPH oxidase requires translocation of the cytosolic components to plasma membranes. ATO treatment induced expression of NADPH oxidase complex subunits P47^{phox}, P67^{phox} and Rac-1 (Fig. 1E.I & 1E.II). ATO also triggered translocation of Rac-1 from the cytosol to plasma membranes, resulting in the formation of catalytically active NOX complex (Fig. 1F). These ATO-mediated changes occurred in $ATF4^{+/+}$ cells, but not in those deficient for the transcription factor. Pretreatment with apocynin, an inhibitor of NADPH oxidase significantly reduced ROS generation in $ATF4^{+/+}$ MEFs treated with ATO (Supplementary Fig. S2), suggesting that the early response of ATO to induce ROS may be mediated by activation of NADPH oxidase pathway. These results demonstrate the importance of ATF4 in ATO-mediated ROS/superoxide production.

3.3. ATO-induced UPR signaling is ATF4-dependent

Following ER stress, ATF4 translocates to the nucleus and initiates the transcription of UPR target genes, including genes encoding additional transcription factors, such as *CHOP* (*GADD153*/*DDIT3*) [23]. Employing immunofluorescence staining of ATF4 and its downstream target CHOP, we determined that both transcription factor translocate from the cytoplasm to nucleus in $ATF4^{+/+}$ MEFs (Fig. 2A & 2B). As expected detection of these transcription factors were much diminished in the $ATF4$-deleted cells. In the UPR, PERK phosphorylation of eIF2α leads to inhibition of protein synthesis and increased translational expression of the transcription factor ATF4 and associated downstream signaling events [24]. Our data confirm that ATO treatment induces p-PERK, GRP78, GRP94, p-eIF2α, and CHOP largely in an ATF4-dependent manner (Fig. 2C.I & 2.C.II). However, following treatment of $ATF4^{-/-}$ MEFs with ATO, the induction of p-eIF2α and CHOP was slightly higher than their respective controls but not as significant as those found in ATO-treated $ATF4^{+/+}$ MEFs. We realize that this slight increase may be indicative of upregulation of additional pathways by ATO. To confirm the role of PERK in ATO-mediated UPR signaling we used ISRIB. ISRIB is a potent inhibitor of PERK signaling by thwarting the ability of eIF2α phosphorylation to trigger global and gene-specific translational control in the UPR [25]. As expected, we found that pharmacological inhibition of the PERK arm of the UPR significantly reduced ATO-induced nuclear translocation of ATF4 (Fig. 2D.I). In addition, we confirmed that ATO-induced CHOP expression was reduced by ISRIB treatment (Fig. 2D.II). Furthermore, UPR inhibitor 4-PBA, attenuated the expression of these proteins,

whereas ER stress inducer thapsiagargin (TG) augmented these effects (Fig. 2E.I & 2E.II). These finding highlight the roles of PERK and ATF4 in the UPR activated by ATO.

3.4. ATF4 is required for ATO-induced ER-mitochondria-mediated apoptosis

Since, ER-stress and mitochondria-regulated signaling pathways represent major pathways for apoptosis, we investigated further the role of ATF4 in the regulation of both of these pathways in cell death. Previously it was reported that activation of IP3R on the ER membrane induces Ca^{++} release from ER to cytosol [26]. The increased cytosolic Ca^{++} induces Ca^{++}/calpain-dependent signaling, leading to apoptosis [27]. Mitochondrial chaperone GRP75 has also been shown to regulate IP3R-mediated mitochondrial Ca^{++} signaling via VDAC [28]. Employing the $ATF4^{+/+}$ and $ATF4^{-/-}$ MEFs, we determined that ATO treatment induces p-IP3R and GRP75 (Fig. 3A), intracellular Ca^{++} release (Fig. 3B.I & 3B.II), and expression of calpain-1, cleaved caspase-12, and cleaved caspase-3 (Fig. 3C.I & C.II) specifically in the cells expressing ATF4. These effects could be inhibited by 4-PBA, a chemical chaperone reported to relieve ER stress, and be augmented by TG treatment (Fig. 3D). To further address the role of Ca^{++} in ATO-mediated cell death, we used a cell permeable calcium chelator, BAPTA-AM [30]. Our results demonstrated that pretreatment of BAPTA-AM significantly blocked ATO-induced cell death in the $ATF4^{+/+}$ MEFs (Fig. 3E). Furthermore, we observed that ATO not only invokes ER stress-regulated Ca^{++}/calpain-mediated apoptosis but also triggers mitochondrial-mediated apoptosis as ascertained by p-p53 (Fig. 4A.I and 4A.II), mROS production (Fig. 4B, Supplementary Fig. S3) and loss of MMP integrity (Fig. 4C). These signals can result in the leakage of cytochrome c from mitochondria to cytoplasm and Bax translocation from cytoplasm to mitochondria in ATF4-dependent manner (Fig. 4D). These results were also confirmed by high resolution confocal microscopy (Fig. 4E).

It is known that a balance of mitochondrial fission and fusion can regulate many mitochondrial functions [19]. In this regard, ATO-treatment of $ATF4^{+/+}$ MEFs induced phosphorylation of dynamin-related protein (DRP1) at Ser 637, and decreased phosphorylation at Ser 616 (Fig. 5A). Drp1, a GTPase family proteins, is associated with several important functional aspects of mitochondria in mammalian cells which include shape and size, distribution, remodeling, and maintenance [31]. In this regard, ATO also induced ultra-structural changes in mitochondria as determined by TEM analysis. The well-defined double membrane structure with high cristae density of mitochondria found in saline-treated control cells (Fig. 5B, panels 1, 2 & 3), were altered in ATO-treated $ATF4^{+/+}$ MEFs (5B, panels 4, 5 & 6). It is also noted that the mitochondria were partially or fully devoid of cristae and showed loss of double membrane structures in response to ATO treatment (Fig. 5B, panels 5 & 6). However, no significant changes in the ultra-structural morphology of mitochondria could be seen in saline-treated vs. ATO-treated $ATF4^{-/-}$MEFs (Fig. 5C, panels 1, 2 & 3 show saline-treated cells and panel 4, 5 & 6 show ATO-treated $ATF4^{-/-}$ cells). Similarly, the proximal organization of ER and mitochondria was also altered in the ATO challenged $ATF4^{+/+}$ cells (Fig. 5D).

In summary, these experiments demonstrate that ATF4 is required for ATO-mediated alterations in both the ER and mitochondria. These results also confirm that ATO-initiated

signals related to protein folding at the ER are important for regulating mitochondrial functions, which can culminate in the control of cell death.

3.5. ATF4 regulates ER-mitochondrial crosstalk following ATO treatment

Previous studies have shown the important effects of arsenic on ER/mitochondrial–mediated apoptosis [8, 11, 12, 32]. However, the role of ATF4 in linking arsenic-mediated ER-mitochondrial crosstalk and -associated cell death were not defined. Our experiments demonstrate that pretreatment of $ATF4^{+/+}$ MEFs with 2-APB, an IP3R channel blocker attenuates ATO-induced phosphorylation of IP3R (Fig. 6A). In addition, 2-APB reduces the ER-regulated Ca^{++}/calpain-1/caspase-12-mediated apoptosis (Fig. 6B) and mitochondrial damage, as determined by the restoration of MMP and diminution of mROS generation in $ATF4^{+/+}$ MEFs (Fig. 6C). Selection of 2-APB in this study was based on a previous report that 2-APB attenuated NMDA-triggered intracellular Ca^{++} increases by blocking IP3R channels and ER stress during neuronal cell death [33]. Furthermore, we also investigated whether VDAC channel inhibitor DIDS, which is known to inhibit Ca^{++} influx into mitochondria [34], affects ATO toxicity. Pretreatment of $ATF4^{+/+}$ cells with DIDS diminished not only the alterations in MMP and mROS production (Fig. 6C) but also thwarted ATO-induced UPR activation (Fig. 6D.I & 6D.II). Interestingly, ISRIB was also found to restore ATO-induced Ca^{++} release (Supplementary Fig. S4) and associated MMP loss as ascertained by JC-1 dye (Fig. 6E). These results support the importance of ER-mitochondria crosstalk in the toxicity of arsenic through a mechanism requiring ATF4.

Discussion

Arsenic is globally distributed toxic metalloid and environmental pollutant [1]. Both *in vitro* and *in vivo* studies have shown that arsenic can induce higher production of ROS, prompting oxidative stress-induced cell damage and subsequent cell death [35, 36]. Recent studies have demonstrated that arsenic-induced oxidative stress has been linked to cell death signaling pathways that include mitochondrial-mediated cell death and ER-regulated cell death [11, 37]. However, the mechanisms regulating these cell death pathways in arsenic toxicity were poorly understood. We show that ATF4 orchestrates the crosstalk between ER and mitochondria as an underlying mechanism of arsenic toxicity. We also demonstrate that ATO-mediated ROS generation is dependent on ATF4.

For these studies we have employed a variety of fluorescent probes. In this regard, DCFH-DA is a widely used probe for detecting intracellular ROS generation in live cells [38]. After passive diffusion into the cell, DCFH-DA is deacetylated by cellular esterases and is oxidized by ROS into 2', 7' –dichlorofluorescein (DCF) which could be detected by fluorescence-based techniques. Nonetheless, use of DCFH-DA is also associated with some artifacts and limitations [39]. For example, direct oxidation of DCFH to DCF by oxidases or cytochrome c could lead to false signal [40-43]. Therefore, our data with DCFH-DA was confirmed with other commercially available ROS/superoxide detection kits. This minimizes the artifacts particularly in the presence of negative controls and various inhibitors. Thus, our data demonstrating that ATO induces O_2^- radical generation in an ATF4-dependent manner involves multiple approaches and supports earlier reports that arsenic induces ROS

[4, 44]. Importantly, we identified NADPH oxidase as the source of ROS generation in cells following ATO insult. ATO-dependent activation of NADPH oxidase requires translocation of the p47^{phox}, p67^{phox} and Rac1 cytoplasmic proteins to plasma membranes via transcriptional activation of *ATF4* as cells devoid of this transcription factor did not show this enzyme assembly. These findings also complement and confirm earlier results showing that *ATF4$^{-/-}$* MEFs following ER or other cellular stress are unable to induce expression of GADD34, a UPR gene associated with cell death following ER stress [45].

CHOP, a gene induced downstream of ATF4 in the UPR, can induce apoptosis during specific ER stress conditions. Sustained activation of CHOP is critical to induce apoptosis [46]. Since we observed that arsenic induces CHOP expression through the PERK/ATF4-dependent pathway, observed apoptosis of *ATF4$^{+/+}$* MEFs is suggested to feature induction of CHOP. However, CHOP also increases ER oxidase 1α (Ero1α) expression, which stimulates calcium release from IP3R on the ER membrane favoring ER Ca^{++} release to cytosol [47]. Therefore, additional mechanisms involving CHOP activation may also contribute to the toxic manifestations of arsenic. Activation of Ca^{++}/calpain-dependent signaling, together with mitochondrial p53-regulated signaling, (Fig. 3 & 4) suggest an important linkage between mitochondrial and cytosolic cell death signaling pathways through processes requiring ATF4.

In summary, blocked IP3R-regulated Ca^{++} release, or reduced mitochondrial Ca^{++} uptake via VDAC inhibition, can attenuate increases in MMP and mROS production and restore cell survival. The findings support the idea that there is an important role of ER-mitochondrial crosstalk in arsenic-mediated toxicity. Our observations that arsenic-induced mitochondrial damage suggest a requirement for this transcription factor in evoking mitochondrial damage and transducing mitochondria-regulated death signals. Further, these studies underscore the importance of ATF4 in the pathogenesis of arsenic toxicity.

Supplementary Material

Refer to Web version on PubMed Central for supplementary material.

Acknowledgments

References

1. Singh R, Singh S, Parihar P, Singh VP, Prasad SM. Arsenic contamination, consequences and remediation techniques: a review. Ecotoxicology and environmental safety. 2015; 112:247–70. [PubMed: 25463877]

2. Hughes MF, Beck BD, Chen Y, Lewis AS, Thomas DJ. Arsenic exposure and toxicology: a historical perspective. Toxicological sciences : an official journal of the Society of Toxicology. 2011; 123(2):305–32. [PubMed: 21750349]

3. Martinez VD, Vucic EA, Becker-Santos DD, Gil L, Lam WL. Arsenic exposure and the induction of human cancers. J Toxicol. 2011; 2011:431287. [PubMed: 22174709]

4. Hunt KM, Srivastava RK, Elmets CA, Athar M. The mechanistic basis of arsenicosis: pathogenesis of skin cancer. Cancer letters. 2014; 354(2):211–9. [PubMed: 25173797]

5. Jomova K, Jenisova Z, Feszterova M, Baros S, Liska J, Hudecova D, Rhodes CJ, Valko M. Arsenic: toxicity, oxidative stress and human disease. Journal of applied toxicology : JAT. 2011; 31(2):95–107. [PubMed: 21321970]

6. Vahter ME. Interactions between arsenic-induced toxicity and nutrition in early life. The Journal of nutrition. 2007; 137(12):2798–804. [PubMed: 18029502]

7. Woo SH, Park IC, Park MJ, Lee HC, Lee SJ, Chun YJ, Lee SH, Hong SI, Rhee CH. Arsenic trioxide induces apoptosis through a reactive oxygen species-dependent pathway and loss of mitochondrial membrane potential in HeLa cells. International journal of oncology. 2002; 21(1):57–63. [PubMed: 12063550]

8. Wang Y, Xu Y, Wang H, Xue P, Li X, Li B, Zheng Q, Sun G. Arsenic induces mitochondria-dependent apoptosis by reactive oxygen species generation rather than glutathione depletion in Chang human hepatocytes. Archives of toxicology. 2009; 83(10):899–908. [PubMed: 19536524]

9. Liu SX, Davidson MM, Tang X, Walker WF, Athar M, Ivanov V, Hei TK. Mitochondrial damage mediates genotoxicity of arsenic in mammalian cells. Cancer research. 2005; 65(8):3236–42. [PubMed: 15833855]

10. Bustamante J, Nutt L, Orrenius S, Gogvadze V. Arsenic stimulates release of cytochrome c from isolated mitochondria via induction of mitochondrial permeability transition. Toxicology and applied pharmacology. 2005; 207(2 Suppl):110–6. [PubMed: 15979664]

11. King YA, Chiu YJ, Chen HP, Kuo DH, Lu CC, Yang JS. Endoplasmic reticulum stress contributes to arsenic trioxide-induced intrinsic apoptosis in human umbilical and bone marrow mesenchymal stem cells. Environmental toxicology. 2016; 31(3):314–28. [PubMed: 25258189]

12. Florea AM, Yamoah EN, Dopp E. Intracellular calcium disturbances induced by arsenic and its methylated derivatives in relation to genomic damage and apoptosis induction. Environmental health perspectives. 2005; 113(6):659–64. [PubMed: 15929885]

13. Walter P, Ron D. The unfolded protein response: from stress pathway to homeostatic regulation. Science. 2011; 334(6059):1081–6. [PubMed: 22116877]

14. Srivastava RK, Li C, Chaudhary SC, Ballestas ME, Elmets CA, Robbins DJ, Matalon S, Deshane JS, Afaq F, Bickers DR, Athar M. Unfolded protein response (UPR) signaling regulates arsenic trioxide-mediated macrophage innate immune function disruption. Toxicology and applied pharmacology. 2013; 272(3):879–87. [PubMed: 23954561]

15. Malhotra JD, Miao H, Zhang K, Wolfson A, Pennathur S, Pipe SW, Kaufman RJ. Antioxidants reduce endoplasmic reticulum stress and improve protein secretion. Proceedings of the National Academy of Sciences of the United States of America. 2008; 105(47):18525–30. [PubMed: 19011102]

16. Leem J, Koh EH. Interaction between mitochondria and the endoplasmic reticulum: implications for the pathogenesis of type 2 diabetes mellitus. Exp Diabetes Res. 2012; 2012:242984. [PubMed: 21785581]

17. Back SH, Kang SW, Han J, Chung HT. Endoplasmic reticulum stress in the beta-cell pathogenesis of type 2 diabetes. Exp Diabetes Res. 2012; 2012:618396. [PubMed: 21915177]

18. Attardi G, Ching E. Biogenesis of mitochondrial proteins in HeLa cells. Methods in enzymology. 1979; 56:66–79. [PubMed: 459888]

19. Darshi M, Mendiola VL, Mackey MR, Murphy AN, Koller A, Perkins GA, Ellisman MH, Taylor SS. ChChd3, an inner mitochondrial membrane protein, is essential for maintaining crista integrity and mitochondrial function. The Journal of biological chemistry. 2011; 286(4):2918–32. [PubMed: 21081504]

20. Pham-Huy LA, He H, Pham-Huy C. Free radicals, antioxidants in disease and health. Int J Biomed Sci. 2008; 4(2):89–96. [PubMed: 23675073]

21. Hordijk PL. Regulation of NADPH oxidases: the role of Rac proteins. Circulation research. 2006; 98(4):453–62. [PubMed: 16514078]

22. Cao SS, Kaufman RJ. Unfolded protein response. Current biology : CB. 2012; 22(16):R622–6. [PubMed: 22917505]

23. Zhang K, Kaufman RJ. Signaling the unfolded protein response from the endoplasmic reticulum. The Journal of biological chemistry. 2004; 279(25):25935–8. [PubMed: 15070890]

24. Teske BF, Wek SA, Bunpo P, Cundiff JK, McClintick JN, Anthony TG, Wek RC. The eIF2 kinase PERK and the integrated stress response facilitate activation of ATF6 during endoplasmic reticulum stress. Molecular biology of the cell. 2011; 22(22):4390–405. [PubMed: 21917591]

25. Sidrauski C, Acosta-Alvear D, Khoutorsky A, Vedantham P, Hearn BR, Li H, Gamache K, Gallagher CM, Ang KK, Wilson C, Okreglak V, Ashkenazi A, Hann B, Nader K, Arkin MR, Renslo AR, Sonenberg N, Walter P. Pharmacological brake-release of mRNA translation enhances cognitive memory. Elife. 2013; 2:e00498. [PubMed: 23741617]

26. Rizzuto R, Marchi S, Bonora M, Aguiari P, Bononi A, De Stefani D, Giorgi C, Leo S, Rimessi A, Siviero R, Zecchini E, Pinton P. Ca(2+) transfer from the ER to mitochondria: when, how and why. Biochimica et biophysica acta. 2009; 1787(11):1342–51. [PubMed: 19341702]

27. Biagioli M, Pifferi S, Ragghianti M, Bucci S, Rizzuto R, Pinton P. Endoplasmic reticulum stress and alteration in calcium homeostasis are involved in cadmium-induced apoptosis. Cell Calcium. 2008; 43(2):184–95. [PubMed: 17588656]

28. Szegezdi E, Logue SE, Gorman AM, Samali A. Mediators of endoplasmic reticulum stress-induced apoptosis. EMBO reports. 2006; 7(9):880–5. [PubMed: 16953201]

29. Orrenius S, Zhivotovsky B, Nicotera P. Regulation of cell death: the calcium-apoptosis link. Nat Rev Mol Cell Biol. 2003; 4(7):552–65. [PubMed: 12838338]

30. Wie MB, Koh JY, Won MH, Lee JC, Shin TK, Moon CJ, Ha HJ, Park SM, Kim HC. BAPTA/AM, an intracellular calcium chelator, induces delayed necrosis by lipoxygenase-mediated free radicals in mouse cortical cultures. Progress in neuro-psychopharmacology & biological psychiatry. 2001; 25(8):1641–59. [PubMed: 11642660]

31. Smirnova E, Griparic L, Shurland DL, van der Bliek AM. Dynamin-related protein Drp1 is required for mitochondrial division in mammalian cells. Molecular biology of the cell. 2001; 12(8):2245–56. [PubMed: 11514614]

32. Yen YP, Tsai KS, Chen YW, Huang CF, Yang RS, Liu SH. Arsenic induces apoptosis in myoblasts through a reactive oxygen species-induced endoplasmic reticulum stress and mitochondrial dysfunction pathway. Archives of toxicology. 2012; 86(6):923–33. [PubMed: 22622864]

33. Ruiz A, Matute C, Alberdi E. Endoplasmic reticulum Ca(2+) release through ryanodine and IP(3) receptors contributes to neuronal excitotoxicity. Cell Calcium. 2009; 46(4):273–81. [PubMed: 19747726]

34. Madesh M, Hajnoczky G. VDAC-dependent permeabilization of the outer mitochondrial membrane by superoxide induces rapid and massive cytochrome c release. The Journal of cell biology. 2001; 155(6):1003–15. [PubMed: 11739410]

35. Ronchetti SA, Bianchi MS, Duvilanski BH, Cabilla JP. In Vivo and In Vitro Arsenic Exposition Induces Oxidative Stress in Anterior Pituitary Gland. Int J Toxicol. 2016

36. Bashir S, Sharma Y, Irshad M, Gupta SD, Dogra TD. Arsenic-induced cell death in liver and brain of experimental rats. Basic & clinical pharmacology & toxicology. 2006; 98(1):38–43. [PubMed: 16433889]

37. Lu TH, Tseng TJ, Su CC, Tang FC, Yen CC, Liu YY, Yang CY, Wu CC, Chen KL, Hung DZ, Chen YW. Arsenic induces reactive oxygen species-caused neuronal cell apoptosis through JNK/ERK-mediated mitochondria-dependent and GRP 78/CHOP-regulated pathways. Toxicology letters. 2014; 224(1):130–40. [PubMed: 24157283]

38. Wojtala A, Bonora M, Malinska D, Pinton P, Duszynski J, Wieckowski MR. Methods to monitor ROS production by fluorescence microscopy and fluorometry. Methods in enzymology. 2014; 542:243–62. [PubMed: 24862270]

39. Kalyanaraman B, Darley-Usmar V, Davies KJ, Dennery PA, Forman HJ, Grisham MB, Mann GE, Moore K, Roberts LJ 2nd, Ischiropoulos H. Measuring reactive oxygen and nitrogen species with fluorescent probes: challenges and limitations. Free radical biology & medicine. 2012; 52(1):1–6. [PubMed: 22027063]

40. Myhre O, Andersen JM, Aarnes H, Fonnum F. Evaluation of the probes 2′,7′-dichlorofluorescin diacetate, luminol, and lucigenin as indicators of reactive species formation. Biochemical pharmacology. 2003; 65(10):1575–82. [PubMed: 12754093]

41. Tarpey MM, Wink DA, Grisham MB. Methods for detection of reactive metabolites of oxygen and nitrogen: in vitro and in vivo considerations. American journal of physiology. Regulatory, integrative and comparative physiology. 2004; 286(3):R431–44.

42. Royall JA, Ischiropoulos H. Evaluation of 2′,7′-dichlorofluorescin and dihydrorhodamine 123 as fluorescent probes for intracellular H2O2 in cultured endothelial cells. Archives of biochemistry and biophysics. 1993; 302(2):348–55. [PubMed: 8387741]

43. Lawrence A, Jones CM, Wardman P, Burkitt MJ. Evidence for the role of a peroxidase compound I-type intermediate in the oxidation of glutathione, NADH, ascorbate, and dichlorofluorescin by cytochrome c/H2O2. Implications for oxidative stress during apoptosis. The Journal of biological chemistry. 2003; 278(32):29410–9. [PubMed: 12748170]

44. Shi H, Shi X, Liu KJ. Oxidative mechanism of arsenic toxicity and carcinogenesis. Molecular and cellular biochemistry. 2004; 255(1-2):67–78. [PubMed: 14971647]

45. Ma Y, Hendershot LM. Delineation of a negative feedback regulatory loop that controls protein translation during endoplasmic reticulum stress. The Journal of biological chemistry. 2003; 278(37):34864–73. [PubMed: 12840028]

46. Iurlaro R, Munoz-Pinedo C. Cell death induced by endoplasmic reticulum stress. The FEBS journal. 2015

47. Tabas I, Ron D. Integrating the mechanisms of apoptosis induced by endoplasmic reticulum stress. Nature cell biology. 2011; 13(3):184–90. [PubMed: 21364565]

Highlights

- ATO-mediated NADPH oxidase complex formation and activation require ATF4.

- ATO-mediated dysregulation of Ca^{++} homeostasis is ATF4 dependent.

- ATO-mediated alterations in mitochondria are ATF4 dependent.

- ER-mitochondrial crosstalk in the toxicity of ATO is regulated by ATF4.
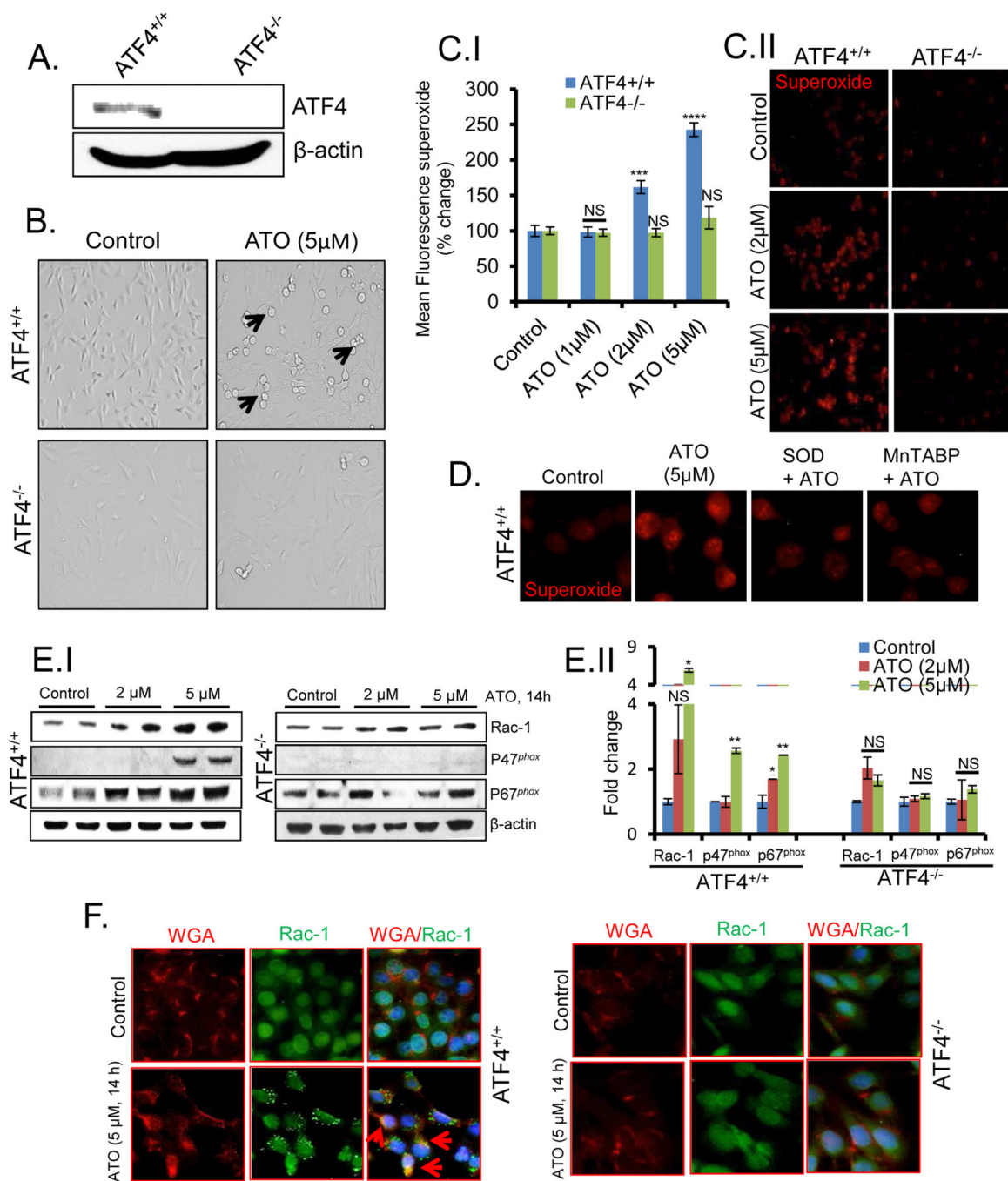
Figure-1. ATO-induced ROS requires ATF4 through activation of NADPH oxidase
(A) Western blot analysis of ATF4 in MEFs. (B) Bright field images of saline (control) and ATO-treated MEFs. ATO-treated cells (5μM, 14h) showing changes in cell rounding, loss of cell adhesion, and blebbing in *ATF4*^{+/+} MEFs (black arrows) but not in *ATF4*^{−/−}. (C.I) Mean fluorescence intensity showing percent change in O_2^- radicals generation in control vs. ATO-treated *ATF4*^{+/+} and *ATF4*^{−/−} MEFs. (C.II) Fluorescence images of superoxide radicals (Red) in *ATF4*^{+/+} and *ATF4*^{−/−} MEFs treated with either saline (control) or ATO. (D) Fluorescence images of ATO-induced superoxide radicals in the absence or presence of SOD

(50 unit/ml, 6 h) or MnTABP (50 μM, 6 h) in $ATF4^{+/+}$ MEFs. O_2^- generation was measured using ROS/superoxide assay kit (Abcam). (E.I) Western blot expression analysis of P67^{phox}, P47^{phox} and Rac-1 in $ATF4^{+/+}$ and $ATF4^{-/-}$ MEFs. (E.II) Histogram showing densitometry analysis of western blots. (F) Immunofluorescence staining of Rac-1 in $ATF4^{+/+}$ and $ATF4^{-/-}$ MEFs. Arrows indicating the translocation of Rac-1 (green) from cytoplasm to the plasma membrane (Red) in ATO-exposed $ATF4^{+/+}$ MEFs. These effects were not observed with $ATF4^{-/-}$ MEFs. Plasma membrane was stained with WGA-conjugated Alexa fluor-594. *P<0.05, **P<0.01, ***P<0.001, ***P<0.0001 compared to their respective controls. NS-Non significant compared to their respective controls.
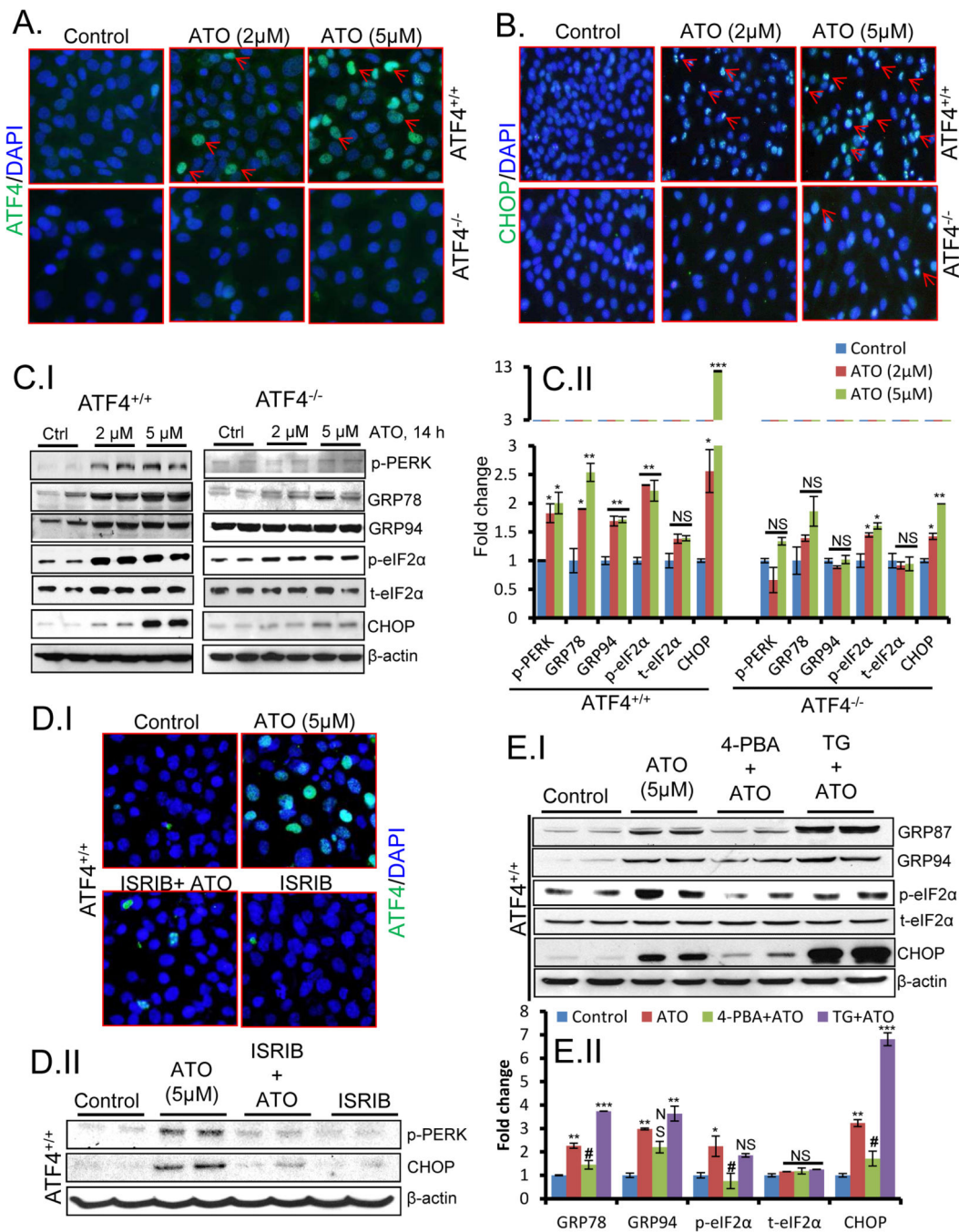
Figure-2. ATO-induced UPR activation requires ATF4

(A & B) Immunofluorescence staining showing nuclear localization of ATF4 (A) and CHOP (B) in ATO-treated *ATF4*$^{+/+}$ MEFs compared to saline-treated control cells. *ATF4*$^{-/-}$ MEFs showed resistance to ATO. Arrows indicate nuclear translocations. Nuclei were stained with DAPI. (C.I) Western blot analyses of UPR signaling proteins p-PERK, GRP78, GRP94, p-eIF2α, t- eIF2α and CHOP in *ATF4*$^{+/+}$ and *ATF4*$^{-/-}$ MEFs. (C.II) Histogram showing densitometric analysis of western blots. (D.I) Pretreatment of ISRIB (250 nM, 6h) significantly blocked ATO-induced nuclear translocation of ATF4 protein in MEFs. (D.II)

Western blot analysis of ATO-induced p-PERK and CHOP in cells pretreated with ISRIB. (E.I) Western blots analysis of GRP78, GRP94, p-eIF2α, total eIF2α, and CHOP in $ATF4^{+/+}$ MEFs pretreated with 4-PBA (1mM) or TG (2.5μM) for 6 h, followed by ATO exposure for 14 h. (E.II) Histograms showing densitometric analyses of western blots. β-actin was used as endogenous control. *P<0.05, **P<0.01, ***P<0.001 compared to their respective controls. #P<0.05 compared to ATO. NS- Non significant compared to their respective controls.
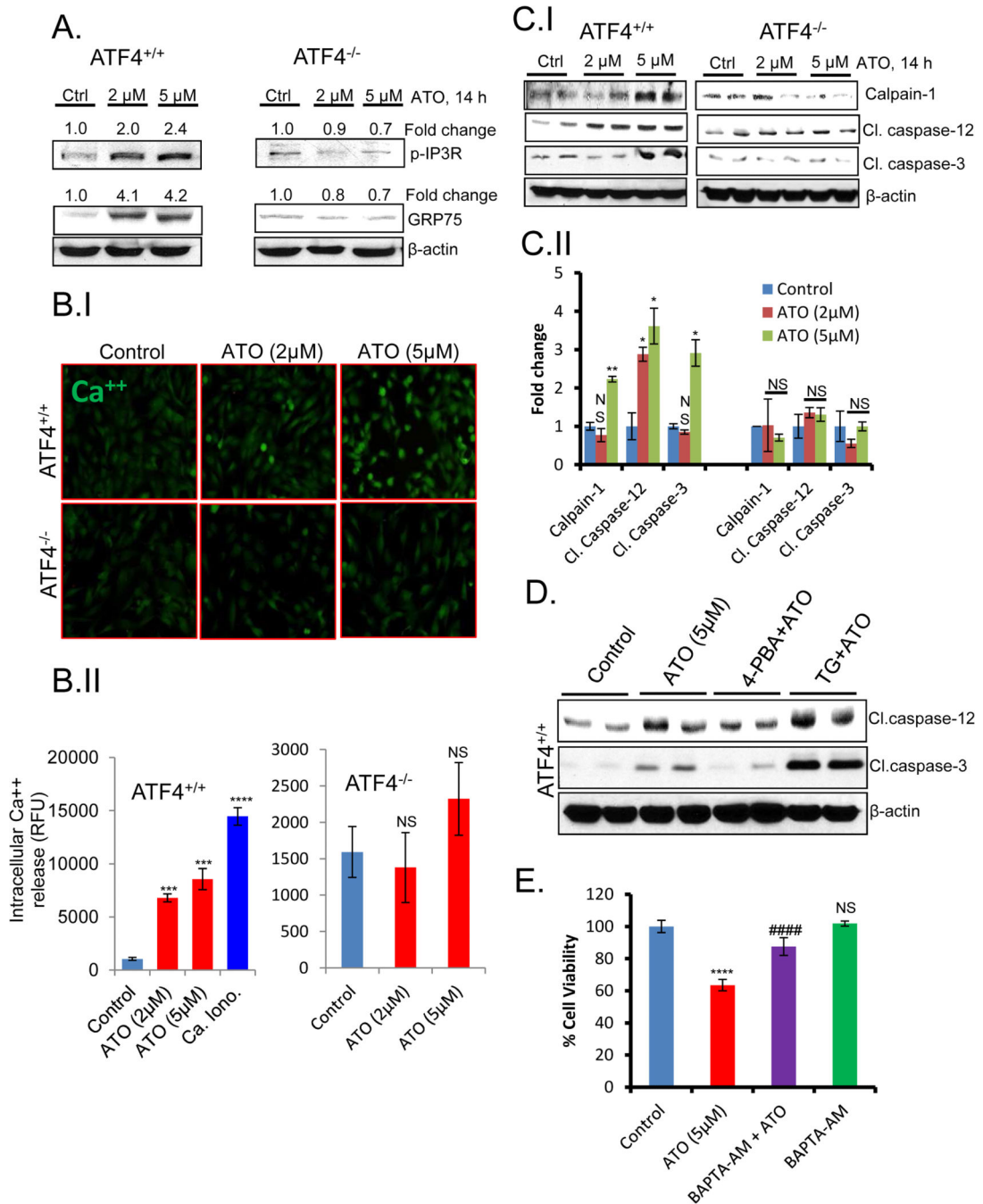
Figure-3. ATO-induced Ca^{++}/calpain-mediated apoptosis is regulated by ATF4

(A) Western blot expression of p-IP3R and GRP75 in either saline-treated (control) or ATO-treated *ATF4$^{+/+}$* and *ATF4$^{-/-}$* MEFs. Protein levels were normalized to endogenous control β-actin and represented as fold change of the indicated proteins. (B.I) Images of *ATF4$^{+/+}$* and *ATF4$^{-/-}$* MEFs showing intracellular Ca^{++} release from MEFs treated with either saline or ATO (2 & 5 μM, 14 h). (B.II) Histograms showing intracellular Ca^{++} release from *ATF4$^{+/+}$* and *ATF4$^{-/-}$* MEFs. Calcium ionophore-A23187 (Ca. Iono.) (2 μM, 3 h) was used as positive control. (C.I) Western blot analyses of calpain-1, cleaved caspase-12 and cleaved

caspase-3 in the cell lysate prepared from MEFs treated with ATF4 or saline (C.II) Histogram showing densitometric analyses of western blots. (D) Western blot measurements of cleaved caspase-12 and cleaved caspase-3. *ATF4*$^{+/+}$ MEFs were pretreated with 4-PBA (1mM) or TG (2.5 μM) for 6 h, followed by ATO exposure for 14 h. (E) Percent cell viability assessed by MTT assays. ATO led to decreased cell viability, which was significantly rescued by pretreatment with BAPTA-AM (5 μM, 6 h). *P<0.05, **P<0.01, ***P<0.001, ***P<0.0001 compared to their respective controls. ###P<0.0001 compared to ATO. NS- Non significant compared to their respective controls.
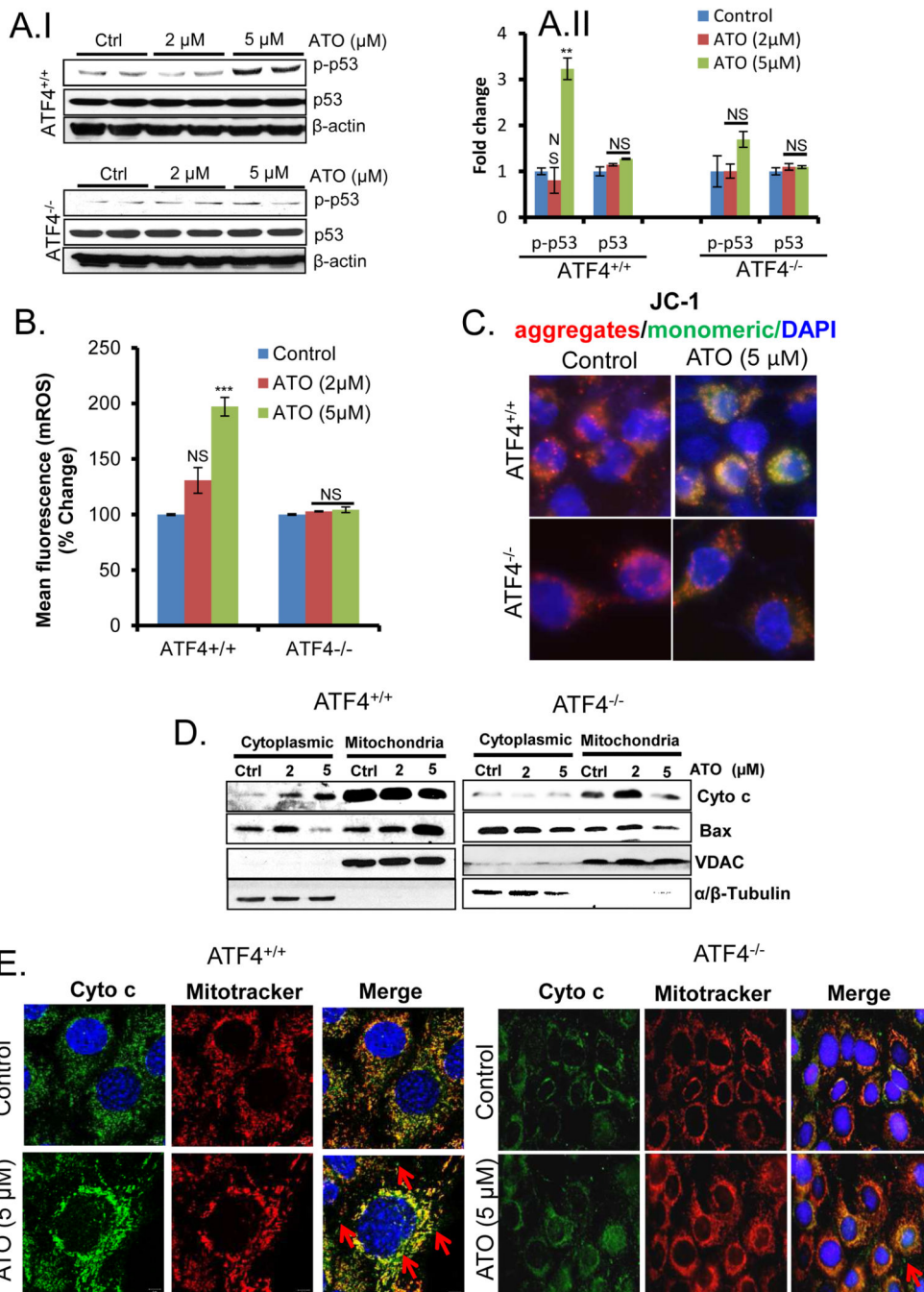
Figure-4. ATO-induced mitochondrial-mediated apoptosis in an ATF4-dependent manner
(A.I) Western blot analyses of phosphorylated p53 (p-p53) and total p53 in *ATF4*^{+/+} and
ATF4^{−/−} MEFs treated with ATO or saline. (A.II) Histograms showing densitometric
measurement of western blots. (B) Mean fluorescence intensity showing percent changes in
mROS generation in saline (control) vs. ATO-treated (5 μM, 14 h) MEFs using Elite™
mROS activity assay kit. (C) Alteration in mitochondrial membrane potential was assessed
using the fluorescent cationic dye, JC-1 (10 μM, 15 min) as assessed by the changes in the
ratio of red (dye aggregates) to green (monomer) forms under a fluorescence microscope in

control vs. ATO-treated (5 μM, 14 h) *ATF4*$^{+/+}$ and *ATF4*$^{-/-}$ MEFs. (D) Western blot analysis of ATO-induced release of cytochrome c (cyto c) from mitochondria to cytoplasm and translocation of Bax from cytoplasm to mitochondria. Fraction purity was confirmed by α/β-tubulin and VDAC for cytoplasmic and mitochondrial fractions respectively. (E) Confocal images of immunofluorescence staining showing release of cytochrome c from mitochondria to cytoplasm in MEFs. ATO-treatment (5 μM, 14 h) releases cytochrome c from mitochondria to cytoplasm (marked by arrows) in *ATF4*$^{+/+}$ MEFs, whereas *ATF4*$^{-/-}$ cells showed significantly diminished release. **P<0.01, ***P<0.01 compared to their respective controls. NS- Non significant compared to their respective controls.
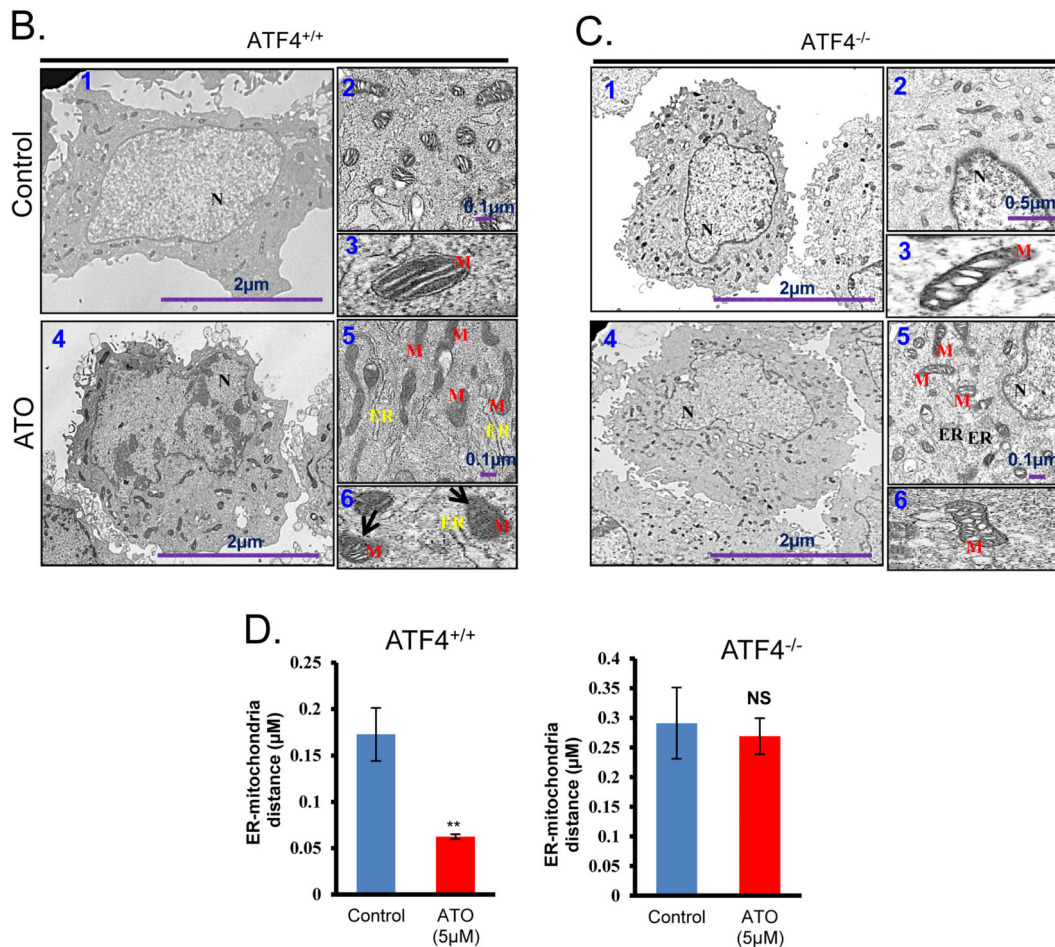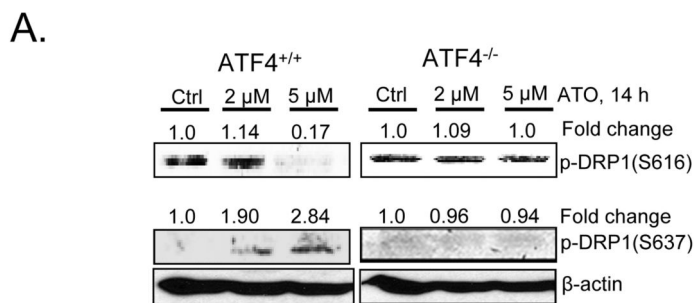
Figure-5. ATO-induced ultrastructural changes in mitochondria are regulated by ATF4
(A) Western blot analyses of phosphorylated-DRP1 (p-DRP1) at S637 and S616 in *ATF4*⁺/⁺
and *ATF4*⁻/⁻ MEFs. Protein levels were normalized to endogenous control β-actin and were
represented as fold changes. (B & C) Saline and ATO (5 μM, 14 h)-treated MEFs were
processed for transmission electron microscopic analysis to assess ultra-structural changes in
mitochondrial morphology. (B) Panel 1, control *ATF4*⁺/⁺ MEFs shows well-maintained
morphology of mitochondria. Panel 2, showing well-organized cristae density. Panel 3,
enlarged image showing well-organized inner and outer membranes of mitochondria. Panel

4, ATO-treated $ATF4^{+/+}$ MEFs shows damaged mitochondria with condensed nuclear material. Panel 5 illustrates elongated mitochondria with the loss of cristae structure, panel 6 showing loss of double membrane structure of mitochondria. (C) Panels 1, 2 and 3 (enlarged image) shows control $ATF4^{-/-}$ MEFs. Panels 4, 5 and 6 (enlarged image) are ATO-treated $ATF4^{-/-}$ MEFs. M, represents mitochondria and ER, indicates endoplasmic reticulum. (D) Morphometric analyses quantifying average distance between ER and mitochondria in ATO-treated and non-treated $ATF4^{+/+}$ and $ATF4^{-/-}$ MEFs. ** $P<0.001$ show significant level. NS- Non significant
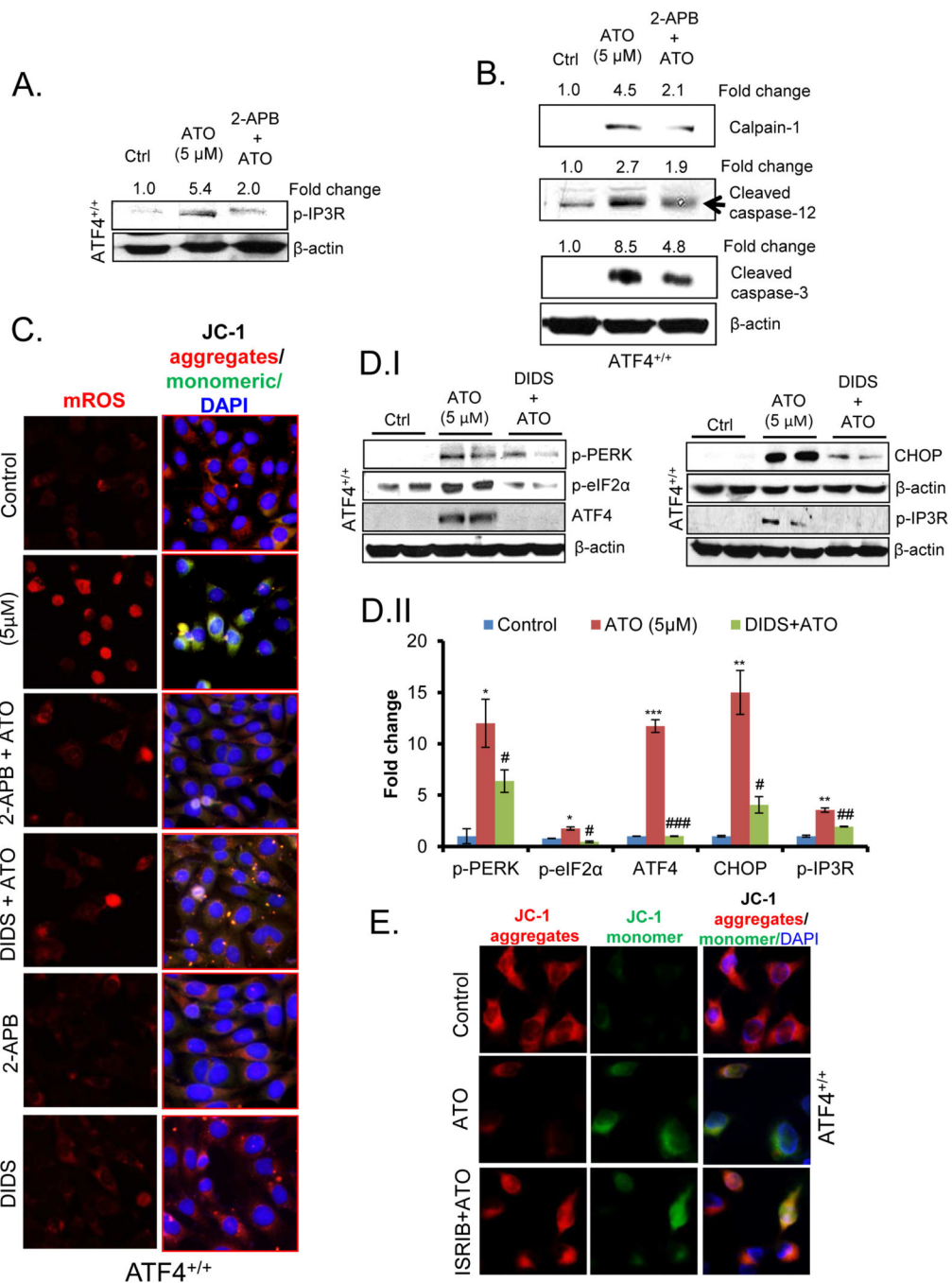
Figure-6. ATF4 promotes ER-mitochondrial crosstalk following ATO treatment
(A & B) Western blot analysis showing levels of p-IP3R, calpain-1, cleaved caspase-12, and cleaved caspase-3 proteins in ATO (5µM, 14h)-treated *ATF4*^(+/+) cells pretreated with either vehicle saline or 2-APB, an IP3R inhibitor. Protein levels were normalized to endogenous control β-actin and represented as fold changes. (C) Alterations in mitochondrial membrane potential and mROS was assessed using a fluorescent cationic dye, JC-1 (10µM, 15min) and Elite™ mROS activity assay kit respectively. Blocking of IP3R and VDAC channel by pretreating *ATF4*^(+/+) cells with 2-APB or DIDS respectively attenuated ATO-induced MMP

and mROS in *ATF4*$^{+/+}$ cells. (D.I) Western blot analyses show pretreatment of *ATF4*$^{+/+}$ MEFs with DIDS reduced the ATO-induced UPR signaling proteins p-PERK, p-eIF2α, ATF4, CHOP, and p-IP3R. (D.II) Histograms showing measurements of proteins analyzed by western blots. (E) MMP was monitored using a fluorescent cationic dye, JC-1 (10 μM, 15 min) as assessed by the changes in the ratio of red (dye aggregates) to green (monomer) forms under the fluorescence microscope. These cells were treated with saline (control) or ATO (5μM, 14 h) or ATO in ISRIB (250nM, 6h) pretreated cells. *P<0.05, **P<0.01, ***P<0.001 compared to their respective controls. #P<0.05, ##P<0.01, ###P<0.001 compared to ATO.